Modelling, fabrication and validation of a high performance 2 DOF piezoactuator for manipulation.

Ricardo Pérez, Joël Agnus, Cédric Clévy, Arnaud Hubert, Nicolas Chaillet

Modeling, Fabrication, and Validation of a High-Performance 2-DoF Piezoactuator for Micromanipulation

Ricardo Pérez, Joël Agnus, Cédric Clévy, Arnaud Hubert, and Nicolas Chaillet

***Abstract*—A high-performance compact micromanipulation system is presented. The system, called the microgripper microrobot on chip (MMOC), was developed at Laboratoire d'Automatique de Besançon (LAB), France. Two main parts in the MMOC design of the MMOC are discussed: 1) the piezoactuator and 2) the end-effectors. The micromanipulator is partially frabricated in a clean room and the piezoactuator system has been machined using the ultrasonic technique. Tests of micromanipulation have been carried out under both standard laboratory conditions as well as inside a scanning electronic microscope (SEM) chamber. Displacements in the plane and out of the plane are 80 and 200 μm, respectively, at 100 V and the MMOC seems to be particularly useful for pick-and-place tasks. Modeling has been performed using the Smits' model and the results confirm the validity of the model for static boundary conditions. The authors have also developed a combined charge and voltage control called Q/V, which results in an order of magnitude reduction in the hysteresis of the piezoactuator. Future work will include integrating force sensors in the micromanipulator in order to measure the manipulation force. This will allow the implementation of the feedback control in the MMOC.**

***Index Terms*—Control, microgripper, micromanipulation, microrobotics, modeling, piezoactuators.**

I. Introduction

MICROMANIPULATION is an emerging research topic with applications in such diverse areas as precision engineering, biology and the watch industry. Each of these areas imposes different physical and technological constraints. For example, adhesion forces are a common issue in the characterization of the micromanipulation in different environments. Miyazaki [1], [2], and Koyano [3] have shown that both adhesion forces and handling skills inside a scanning electron microscope (SEM) chamber have to take into account in order for micromanipulators to accomplish different tasks. In addition, good force resolution is necessary to assure the success of the manipulation task.

The design and characterization of the micromanipulator are crucial steps in determining its performance. The choice of the actuation principle for the manipulator, the materials selected, the dimensions and flexibility of the system to be integrated into other complex devices must all be carefully considered from the engineering point of view.

Piezoelectric materials are a good choice for systems such as micromanipulators due to their fast reaction times and miniaturization possibilities [4]. This is the case of the microgripper microrobot on chip (MMOC) proposed by the Laboratoire d'Automatique de Besançon (LAB), France. The MMOC is the result of several years of research on piezoactuators. This study covers characterization and control of piezoactuators. Previous developments in control have been utilized in this work and the results demonstrate the convenience of such approach. The MMOC has a simple design and the ability to be integrated in other systems.

This work presents the fabrication, modeling, characterization of the MMOC as well as micromanipulation tests performed with the device. Section II presents the working principle of the MMOC. Section III deals with the fabrication of the MMOC. Modeling of the piezoactuator system will be presented in Section IV while Section V describes the modeling of the whole micromanipulator system. The characterization of the MMOC and micromanipulation tests carried out in the laboratory will be presented in Section VI. The control method applied to the micromanipulator will be presented in Section VII. Section VIII contains the conclusions and opportunities for future study.

II. MMOC Micromanipulator

The MMOC is a compact micromanipulator. Two main components in the design of this micromanipulator are: 1) the piezoactuator and 2) the end-effectors (see Figs. 1 and 3). The piezoactuator system consists of a single two-layer piezoceramic plate. It consists of two parallel bimorphs and is machined using an ultrasonic technique (sonotrode). The end-effectors used to handle microobjects are made of nickel (Ni) and are machined using the LIGA (X-ray lithography) technique. Assembly of the piezoactuator system and end-effectors results in a MMOC micromanipulator. While the piezoceramic system is active, the end-effectors are passive and are responsible for the micromanipulation. Fig. 1 shows a detail of the piezoceramic actuator (left) and the nickel end-effectors (right) used in the MMOC configuration.

The piezoactuator system is made of a soft piezoceramic. Each parallel bimorph is independent and has two degrees of freedom (DoF). The thickness of the piezoceramic bimorph is 400 μm with an electrode length of 13 mm. The end-effectors are 200 μm thick with an initial gap of 250 μm between the fingers.

Manuscript received December 30, 2003; revised December 13, 2004. This work was supported in part by the Robosem project (GRD1-2001-41861) of the European Union.

The authors are with the Laboratoire d'Automatique de Besançon (LAB), Besançon 25000, France (e-mail: ricardo.perez@ ens2m.fr).

Digital Object Identifier 10.1109/TMECH.2005.844712

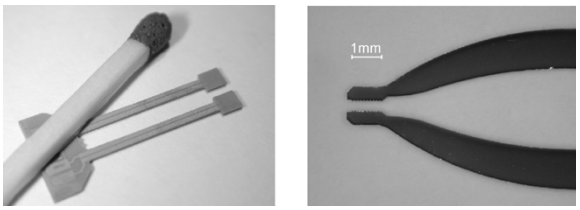

Fig. 1. Piezoceramic actuator (left) and end-effectors (right) as main components of the MMOC. The end-effectors are LIGA made and the piezoceramic is machined with an ultrasonic cutting device.

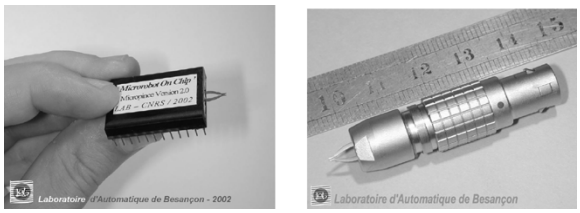

Fig. 2. Two versions of microgripper MMOC (left) and LEMMOC (right). The example on the left is the first packaging version. The LEMO version on the right is much more compact and has the same performance.

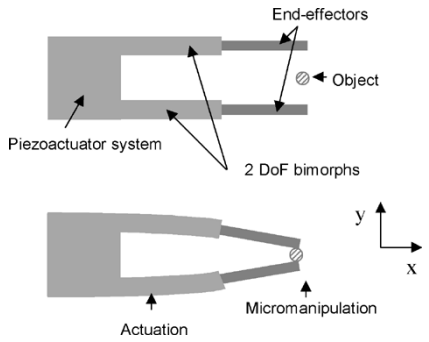

Fig. 3. General micromanipulator is composed by a piezoactuator system and end-effectors as those of the MMOC. In this case the actuation is made in the x-y plane.

The assembly of the piezoactuator system and end-effectors gives a very compact and flexible configuration, which can be easily integrated in complex systems such as micromanipulation platforms. Fig. 2 shows two versions of the MMOC packaging for micromanipulation tasks.

One of the main advantages of the micromanipulator configuration shown in Fig. 3 is the compactness. A second advantage for micromanipulation tasks is the possibility of actuation in the x–y plane (as shown in the figure) or out from the x–y plane (z axis) with this single structure.

III. Fabrication

The fabrication process of a MMOC is presented in Fig. 4. The whole process is carried out in grey and clean rooms. Typically, the assembly, machining, and packaging steps are not preformed in a clean room.

Soft piezoceramic plates (PIC 151) are used for the fabrication process. This piezoceramic is well adapted to the application requirements of the microgripper where quasi-static working conditions and large displacements are required. This piezoceramic has a coupling coefficient $k_{31} = 0.34$ and a piezoelectric charge coefficient $d_{31} = -210 \times 10^{-12}$ CN^{-1} [8].

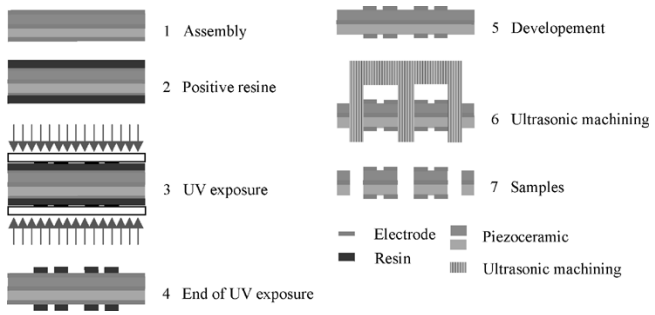

Fig. 4. Steps of the fabrication of the piezoactuator system of the MMOC using a soft piezoceramic PIC151.

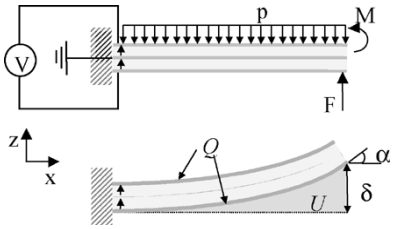

Fig. 5. Bimorph piezoactuator under different electromechanical constraints defined in the Smits' model.

After the bonding of two piezoceramic layers using a conductive epoxy glue (step 1), a resin is applied on the electrode surface (step 2) before carrying out the photolithography (steps 3–5). The electrode pattern is defined for the design of the piezoactuator in the masks (step 3). After development by UV exposure (step 5), the resulting plate is ready to be machined. Machining of the piezoactuator system for the micromanipulator is performed using an ultrasonic machining technique [9], [10], with the advantage of having low impact on the material properties of the piezoceramic substrate.

Fabrication tolerances play an important role in the performance of the micromanipulator. Generally, two main sources can be differentiated. The first is the alignment of electrodes of two bimorphs that can be highly affected by the tolerances during the photolithography. This misalignment can decrease the performance of the microgripper through the introduction of undesirable parasitic displacements. The second source of error is the machining of prototypes from the piezoceramic plate using the ultrasonic technique.

IV. Modeling of a Bimorph Piezoactuator

The model of the piezoactuator system presented in this section aims to determine the fundamental parameters such as displacement or deflection angle depending upon the boundary conditions applied to the bimorph piezoactuator. The Smits' model [11] is used to accomplish this task. It consists of a set of equations that are used to calculate parameter magnitudes related to a bimorph piezoactuator under electromechanical constraints as shown in Fig. 5.

The output magnitudes in the Smits' model are angle α, flection δ, removed volume U, and charge Q under mechanical or electrical constraints such as bending moment M, force F, pressure p, and voltage V. Equation (1) shows the matrix form of the

TABLE I
COEFFICIENTS FOR THE z-MODE

a_{ij}	$i=1$	$i=2$	$i=3$	$i=4$
$j=1$	$\frac{3s_{11}^E l}{2wh^3}$	$\frac{3s_{11}^E l^2}{4wh^3}$	$\frac{s_{11}^E l^3}{4h^3}$	$-\frac{3d_{31}l}{2h^2}$
$j=2$	$\frac{3s_{11}^E l^2}{4wh^3}$	$\frac{s_{11}^E l^3}{2wh^3}$	$\frac{3s_{11}^E l^4}{16h^3}$	$-\frac{3d_{31}l^2}{4h^2}$
$j=3$	$\frac{s_{11}^E l^3}{4h^3}$	$\frac{3s_{11}^E l^4}{16h^3}$	$\frac{3ws_{11}^E l^5}{40h^3}$	$-\frac{d_{31}wl^3}{4h^2}$
$j=4$	$-\frac{3d_{31}l}{4h^2}$	$-\frac{3d_{31}l}{4h^2}$	$-\frac{d_{31}wl^3}{4h^2}$	$\frac{2\varepsilon_{33}^T lw(1-k_{31}/4)}{h}$

general Smits' model. Index i means the z- or y-mode, respectively

$$\begin{pmatrix}\alpha\\ \delta\\ U\\ Q\end{pmatrix}_i = \begin{bmatrix}a_{11} & a_{12} & a_{13} & a_{14}\\ a_{21} & a_{22} & a_{23} & a_{24}\\ a_{31} & a_{32} & a_{33} & a_{34}\\ a_{41} & a_{42} & a_{43} & a_{44}\end{bmatrix}_i \begin{pmatrix}M\\ F\\ p\\ V\end{pmatrix}_i. \quad (1)$$

Coefficients a_{ij} are calculated according to Smits *et al.* [11] from the piezoelectric equations, the bending moment balance equation and the internal energy balance

$$S_1 = s_{11}^E T_1 + d_{31}E_3 \quad (2)$$

$$D_3 = d_{31}T_1 + \varepsilon_{33}E_3 \quad (3)$$

$$\iint T_1(x,y,z)ydA + M_z = 0 \quad (4)$$

$$u = \frac{1}{2}s_{11}^2 T_1^2 - d_{31}E_3T_1 + \frac{1}{2}\varepsilon_{33}^T E_3^2. \quad (5)$$

S_1 is the strain, s_{ij} the compliance coefficient, T_1 the mechanical stress, d_{ij} the charge piezoelectric coefficient, E_3 the electric field, D_3 the charge density, and ε_{33} the electric permittivity. Coefficients for the z mode obtained by Smits *et al.* are presented in Table I.

The basic working principle of a single finger in the piezoactuator system is the principle of a parallel bimorph. A unique feature of this bimorph is that it has two DoF. Fig. 6 shows the geometrical configuration of this piezoactuator. The output displacements δ_y and δ_z at the output of the beam are also represented.

Fig. 7 shows the working principle of the geometrical configuration of Fig. 6. Applying a voltage V_z results in the output displacement δ_z as pictured in Fig. 7(a).

Displacement δ_y results from the application of a voltage V_y and $-V_y$ in a cross configuration on the electrodes. Cases a and b will be called hereafter z-mode and y-mode, respectively. A third working configuration is possible if voltages V_z and V_y are applied simultaneously on the electrodes. The output displacement δ_{yz} is a coupled displacement between the y- and z-mode as shown in Fig. 7(c).

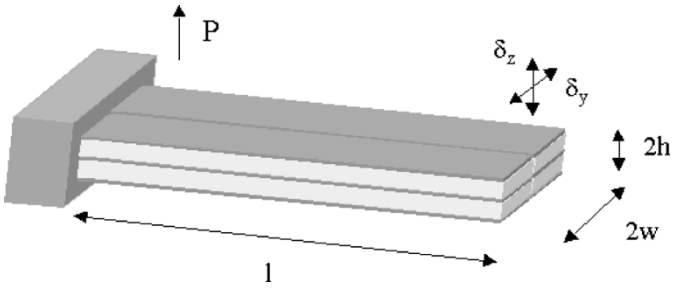

Fig. 6. Geometrical configuration of the duo-bimorph used for the micromanipulator. Displacemen in the z and y axis are possible thanks to the design.

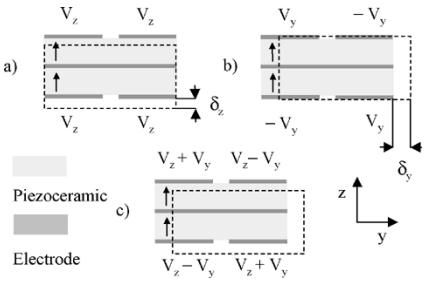

Fig. 7. Working principle of the duo-bimorph with the electric configuration resulting in displacements δ_y, δ_z and a combination of both.

TABLE II
COEFFICIENTS FOR THE y-MODE

a_{ij}	$i=5$	$i=6$	$i=7$	$i=8$
$j=5$	$\frac{12s_{11}^E l}{hw^3}$	$\frac{6s_{11}^E l^2}{hw^3}$	$\frac{2s_{11}^E l^3}{hw^3}$	$-\frac{3d_{31}l}{4hw}$
$j=6$	$\frac{6s_{11}^E l^2}{hw^3}$	$\frac{4s_{11}^E l^3}{hw^3}$	$\frac{3s_{11}^E l^4}{hw^3}$	$-\frac{3d_{31}l^2}{4hw}$
$j=7$	$\frac{2s_{11}^E l^3}{hw^3}$	$\frac{3s_{11}^E l^4}{2hw^3}$	$\frac{3s_{11}^E l^5}{5hw^3}$	$-\frac{3d_{31}l^3}{4hw}$
$j=8$	$-\frac{3d_{31}l}{4w^2}$	$-\frac{3d_{31}l^2}{8w^2}$	$-\frac{d_{31}hl^3}{4w^2}$	$\frac{\varepsilon_{33}^T lw(1-k_{31}/4)}{2w}$

In a previous work [12], the authors have presented an extension of the Smits' model to obtain coefficients a_{ij} for the y-mode. In that work, however, de Lit *et al.* [12] did not calculate coefficients a_{ij} for $j=4$ and $i=\{1,2,3,4\}$ concerning the charge Q as the result of the M, F, p, and V. These coefficients have now been calculated following the Smits' approach and are outlined in Table II.

Actuation in y- and z-mode can be written in a compact form shown in (6). No coupling between the y- and z-mode is considered in this case

$$\begin{pmatrix}\alpha_y\\ \delta_y\\ U_y\\ Q_y\\ \alpha_z\\ \delta_z\\ U_z\\ Q_z\end{pmatrix} = \begin{pmatrix}a_{11} & a_{12} & a_{13} & a_{14} & 0 & 0 & 0 & 0\\ a_{21} & a_{22} & a_{23} & a_{24} & 0 & 0 & 0 & 0\\ a_{31} & a_{32} & a_{33} & a_{34} & 0 & 0 & 0 & 0\\ a_{41} & a_{42} & a_{43} & a_{44} & 0 & 0 & 0 & 0\\ 0 & 0 & 0 & 0 & a_{55} & a_{56} & a_{57} & a_{58}\\ 0 & 0 & 0 & 0 & a_{65} & a_{66} & a_{67} & a_{68}\\ 0 & 0 & 0 & 0 & a_{75} & a_{76} & a_{77} & a_{78}\\ 0 & 0 & 0 & 0 & a_{85} & a_{86} & a_{87} & a_{88}\end{pmatrix} x \begin{pmatrix}M_z\\ F_y\\ p_y\\ V_y\\ M_y\\ F_z\\ p_z\\ V_z\end{pmatrix}. \quad (6)$$

An important working parameter of piezoactuators is the blocking force needed to cancel the displacement generated when a voltage V is applied as shown in Fig. 5

$$F_z = \frac{3d_{31}hw}{2s_{11}^E L}V \tag{7}$$

$$F_y = \frac{3d_{31}w^2}{16s_{11}^E L}V. \tag{8}$$

The ratio between blocking forces in y- and z–mode depends only upon the geometry. For bimorph configurations, such as that used for the MMOC, the ratio between width and thickness is $w \approx 5h/2$

$$\frac{F_z}{F_y} = \frac{8h}{w}. \tag{9}$$

Another important parameter from the modeling point of view is the evaluation of the mechanical coupling and the efficiency of the bimorph system. According to Wang *et al.* [13], the coupling coefficient of the piezoelectric bimorph in z configuration is calculated according to

$$k_z = \frac{9}{16}\left(\frac{k_{31}^2}{1-\frac{k_{31}^2}{4}}\right). \tag{10}$$

The coupling coefficient of the piezoactuator is defined as the ratio between the mechanical energy output and the electrical energy input as: $k = Emec/E_{elec}$. The electrical and mechanical energy are defined according to Wang [13] as $Emec = (1/2)(\varepsilon_{33}lw(1-k_{31}^2/4)/h)V$ and $Emec = (9/32)(d_{31}^2/s_{11}^E)(lw/h)V^2$.

The coupling coefficient k_{31} is calculated according to the standard equation and it is a function of the intrinsic parameters of the piezoceramic [14]

$$k_{31}^2 = \frac{d_{31}^2}{\varepsilon_{33}^T s_{11}^E}. \tag{11}$$

The coupling coefficient related to the y-mode is calculated in the same way as that for the z-mode

$$k_y = \frac{9}{64}\left(\frac{k_{31}^2}{1-\frac{k_{31}^2}{4}}\right). \tag{12}$$

In comparing k_y and k_z, it is found that k_z is four times larger than k_y. This result is expected if we take into account that the stiffness is higher for the y-mode and consequently the mechanical energy produced for a given electrical energy input is smaller. This result must be taken into account for working and design purposes.

V. Static Model of the Micromanipulator

A simplified model of one finger of the micromanipulator is considered in Fig. 8(a). This model takes into account only one finger of the micromanipulator system shown in Fig. 3.

The piezoelectric actuator and the end-effector are represented as piezoelectric and metallic beams, respectively. They are defined by length $L_{\rm PZT}$ for the piezoelectric beam and length $L_{\rm EE}$ for the end-effector. Both beams have their own material properties including the compliance s_{11} and, in the case of the piezoceramic beam, the piezoelectric charge coefficient d_{31}.

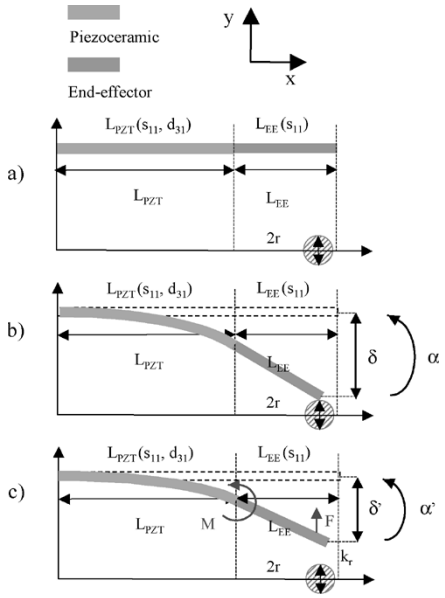

Fig. 8. Simplified model of a micromanipulator used in the analytical and FE models. The active and nonactive parts represent the piezoceramic and the end-effector, respectively.

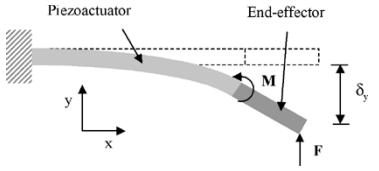

Fig. 9. Micromanipulation system with active part, piezoactuator, and passive part, end-effector. A force F is applied on the tip of the end-effector generating a bending moment M.

When a voltage V is applied to the bimorph, the piezoceramic beam bends and the end-effector rotates without deformation as shown in Fig. 8(b). This is the case of one gripper of the micromanipulator shown in Fig. 8(c). The whole system can be scaled according to the magnitude of force F and the diameter a of the object to be handled.

Equations used to calculate deflection δ_y correspond to those given by de Lit [12] for the y-mode. When a voltage V is applied, bending of the whole structure takes place. If a force F is applied on the end-effector, a bending moment M on the bimorph beam will appear as shown in Fig. 9.

The present model has been applied to the configuration of a 2-DoF microactuator. Nevertheless, it can also be applied to the study of micropositioning and scanning tasks, for example.

The flection function δ_y and output angle α_y for the whole system (piezoactuator and end-effector) when no force on the end-effector tip is applied is calculated from the previous model as follows in (13). The superscript PZT indicate parameters concerning the piezoelectric beam

$$\delta_y(x) = \begin{cases} 0 < x \le L_{\rm PZT}, & \delta_y^{\rm PZT}(x) \\ L_{\rm PZT} < x \le L_{\rm EE}, & \delta_y^{\rm PZT}(L_{\rm PZT}) + \alpha_y^{\rm PZT}(L_{\rm EE})\cdot x \end{cases}. \tag{13}$$

where δ_y^{PZT} and α_y^{PZT} can be calculated from the following equations:

$$\delta_y^{\mathrm{PZT}} = -\frac{3d_{31}V}{4hw}x^2 \tag{14}$$

$$\alpha_y^{\mathrm{PZT}} = -\frac{3d_{31}V}{4hw}x. \tag{15}$$

When a force F is applied on the end-effector, the new flection function δ_y^F becomes (16), shown at the bottom of the page.

Superscript $^{\mathrm{PZT,F}}$ indicates flexion of the PZT beam under force F applied on the end-effector. In this case, flexion δ_y^F of the piezoceramic beam is due to the voltage and the bending moment as shown in the following equations:

$$\delta_y^{\mathrm{PZT,F}} = -\frac{3d_{31}V}{4hw}x^2 + \frac{6s_{11}^E M}{hw^3}x. \tag{17}$$

The output angle α after applying force F is calculated then from the general model as shown in the following equation:

$$\alpha_y^{\mathrm{PZT,F}} = -\frac{3d_{31}L_{\mathrm{PZT}}^2}{2hw}V + \frac{12s_{11}^E L}{hw^3}M. \tag{18}$$

The bending moment M applied at the end of the piezoelectric beam is calculated from the classical mechanics equation

$$M = F_{\mathrm{EE}}L_{\mathrm{EE}}. \tag{19}$$

Equations (12)–(18) permit the assessment of the influence of interaction forces on the micromanipulation system. Force F is supposed to be opposite to the bending due to the voltage. This means that expected output flection at the end of the end-effector is less than in the free case [Fig. 7(b)]

$$\delta_z(L_{\mathrm{EE}}) > \delta_z^F(L_{\mathrm{EE}}). \tag{20}$$

Fig. 10 shows the effect of the reaction forces on the deflection δ_y of finger according to Fig. 9. The blocking force F_b can be considered as a reference limit. Reaction forces when handling are in general much smaller than F_b and depend on object to be handled. A rough approach of the order of interaction forces in the micromanipulator is $F_r \approx c\,F_b$ where constant c has to be determined for each particular case of manipulation.

A force of 50 mN for instance reduces the free voltage bending δ_y of 15% according to the results of the analytical model developed in this section. For the present case, the blocking force can be calculated from (21). The condition to calculate the blocking force comes from the equation

$$\delta_y^{\mathrm{PZT,F}} + \alpha_y^{\mathrm{PZT,F}}(L_{\mathrm{EE}} + \delta_y^{\mathrm{EE,F}}) = 0. \tag{21}$$

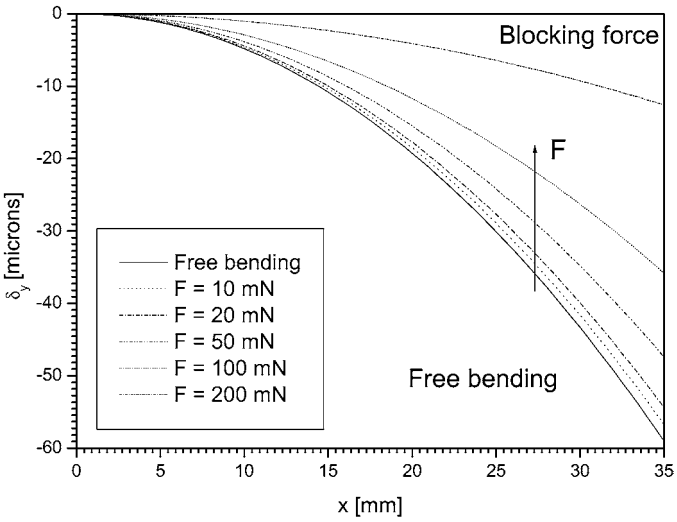

Fig. 10. Variation of the deflexion δ with the reaction force F. The limit is given by the x axis ($\delta = 0$), which represents the blocking force of the whole system, bimorph and end-effector.

The last equation can be simplified under the approximation that $\alpha_y^{\mathrm{PZT,F}}$ and $\delta_y^{\mathrm{EE,F}}$ are sufficiently small and consequently the product $\alpha_y^{\mathrm{PZT,F}}\delta_y^{\mathrm{EE,F}}$ can be neglected. The remaining equation for the blocking force condition is

$$\delta_y^{\mathrm{PZT,F}} + \alpha_y^{\mathrm{PZT,F}}L_{\mathrm{EE}} = 0. \tag{22}$$

Substituting from (17) and (18)

$$F_b = \frac{w^2 L_{\mathrm{PZT}}d_{31}V}{4s_{11}^E L_{\mathrm{EE}}}\frac{(1+L_{\mathrm{EE}})}{(1+2L_{\mathrm{EE}})}. \tag{23}$$

The last equation is similar to the precedent equations for the blocking forces in z- and y-modes. The main difference is the ratio between the piezoceramic and end-effector lengths L_{PZT} and L_{EE}.

VI. Characterization of the Micromanipulator

Characterization of a MMOC micromanipulator has been done with samples shown in Fig. 2 in two different environments: the laboratory and SEM chamber. Results obtained in both cases are quite close and no influence of the environment on the performance of the MMOC has been observed. Output displacements of the micromanipulator are 200 μm outside the x-y plane (called z axis) and 80 μm in the x-y plane (called y axis) at 100 V. Fig. 11 shows the hysteresis loop of the tip of the end-effector and the theoretical value expected. Measurements are quite close to the theoretical values obtained with the proposed model in Sections IV and V. Hysteresis measured in

$$\delta_y^F(x) = \begin{cases} 0 < x \le L_{\mathrm{PZT}}, & \delta_y^{\mathrm{PZT,F}}(x) \\ L_{\mathrm{PZT}} < x \le L_{\mathrm{EE}}, & \delta_y^{\mathrm{PZT}}(L_{\mathrm{PZT}}) + \alpha_y^{\mathrm{PZT}}(L_{\mathrm{PZT}})\cdot x + \alpha_y^{\mathrm{PZT}}(L_{\mathrm{PZT}})\delta_y^{\mathrm{EE}}(x) \end{cases} \tag{16}$$

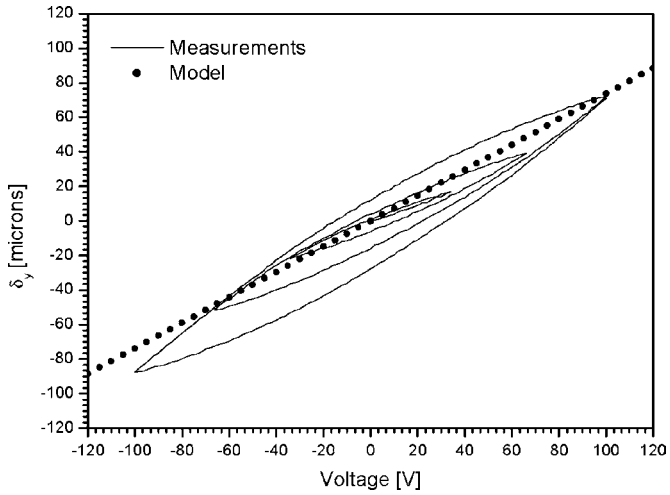

Fig. 11. Variation of the deflection δ_y versus the applied voltage V for a piezoactuator beam. Results from the model (dots) and hysteresis loops measured in the laboratory are plotted.

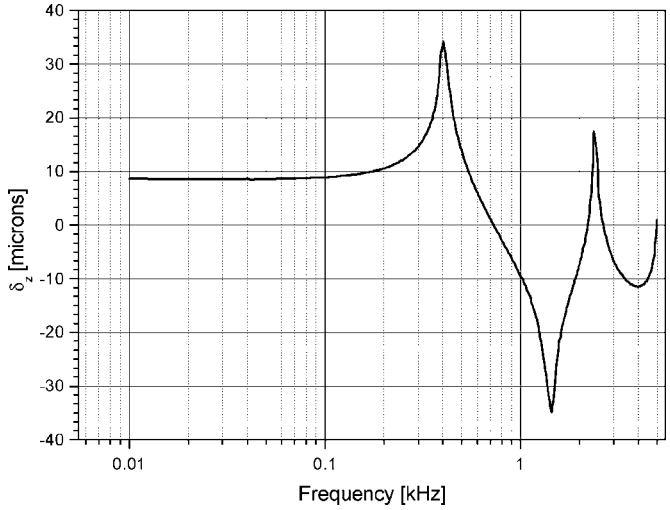

Fig. 12. Variation of the deflection δ_z with the frequency. The first resonance frequency is situated at 400 Hz.

the laboratory for this case is 24.6%. Similar values have been measured in the SEM chamber.

Frequency characterization has also been performed in the laboratory and the results are shown in Fig. 12. The first bending mode outside the x-y plane corresponds to 400 Hz. The bandwidth estimated from the results is 100 Hz for the MMOC version shown in Fig. 2.

VII. Control

Preliminary results concerning a charge control for the displacements of piezoactuators in open loop have been proposed by the authors in a previous work [15]. We propose to describe in this section a control method based on the combination of constant charge control and constant voltage control. An important reduction of the hysteresis, up to one order of magnitude less than the nominal value of the hysteresis, is obtained by this method.

Piezoactuators are generally controlled using either an open loop with voltage control input or a closed loop with a position

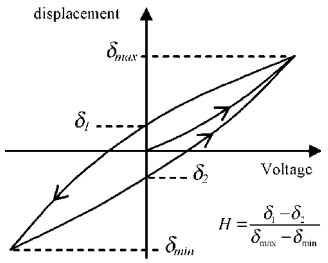

Fig. 13. Hysteresis loop of a piezoceramic for a displacement voltage representation.

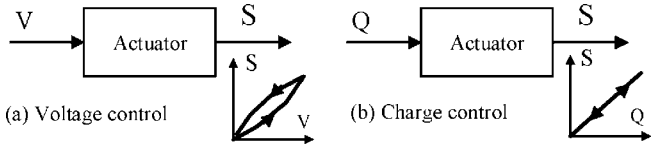

Fig. 14. Control principles of piezoelectric actuators. V and Q are, respectively, the voltage and the electrical charge applied on the piezoactuator, ε is the strain of the material.

set point and an applied voltage on the actuator. The first case consists of a simple control in which a voltage is applied to the terminals of the piezoactuator. The main disadvantage of this method is the nonlinearity between the deformation (position) and voltage. Typical values of hysteresis for a soft piezoceramic can reach 20%. Fig. 13 shows the hysteresis loop of a piezoceramic for a displacement (δ)–voltage representation.

Due to the lack of precision in the displacement δ, three different solutions can be used. The first consists of implementing a position servomechanism. This method is very efficient, but it is also very expensive because of the position sensor and the appropriate regulation system required. Another solution to this problem is the implementation of linear control based on the behavior of inverse models such as those of Preisach [16] and Maxwell [17]. The disadvantage of this approach is the lack of robustness of the linearization when the model is applied to different kinds of piezoactuators. A third solution consists in using a compliance feedback charge driver [18], [19], which offers less hysteresis than voltage control and compensates for charge losses. This method gives low-frequency bandwidths in the megahertz range but the proposed control method can keep the position in static conditions that could be needed within positioning applications.

A. Control With Constant Charge

Generally, piezoactuators are controlled with the applied voltage due to the ease of implementation of such a system. Nevertheless, the electromechanical transfer between the applied voltage and the strain is not linear. Hence, the strain is not the proportional as the voltage increases and decreases [see Fig. 14(a)]. Another control option consists of using a charge control [see Fig. 14(b)]. As a result, a constant quantity of free electrical charges is applied on the electrodes of the piezoactuator. This control method results in a more linear behavior between the applied charge and the strain.

Equations (24) and (25) can be used to explain the difference between the voltage and charge control methods. Under no external stress ($T_q = 0$), (2) (see Section IV) indicates that the

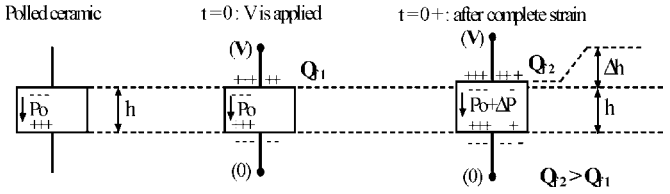

Fig. 15. Phenomenology of the charge control on the quantity of free charges on the electrodes of a piezoceramic with polarization P_o and thickness h.

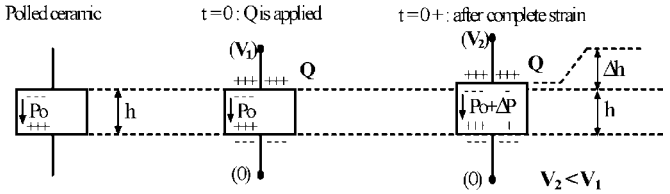

Fig. 16. Phenomenology of charge control of a piezoceramic with polarization P_o and thickness h.

strain S_p is proportional to the electric field E_k. For the elongation of a planar piezoceramic structure, S_1 can be written by substitution of E_k from (24) and (25) as follows:

$$S_1 = \left(s_{11}^E - \frac{d_{31}^2}{\varepsilon_{33}^T}\right) \cdot T_1 + \frac{d_{31}}{\varepsilon_{33}^T} \cdot D_3. \tag{24}$$

The Gauss law allows determination of the free charge quantity on the electrodes of the piezoceramic as follows:

$$\int_{\text{Surface}} D \cdot ds = Q_f \Rightarrow Q_f = D_3 \cdot A \tag{25}$$

where A is the surface of the electrode. Substituting D_3 from (25) into (24), we obtain the linear equation of the strain linked to the stress T_1 and the free charges Q_f as

$$S_1 = \left(s_{11}^E - \frac{d_{31}^2}{\varepsilon_{33}^T}\right) \cdot T_1 + \frac{d_{31} \cdot Q_f}{\varepsilon_{33}^T \cdot A}. \tag{26}$$

Fig. 15 shows the result when a constant voltage V is applied on the electrodes of a piezoactuator. If a polled ceramic (P_o) with a thickness h is considered and a voltage V is applied at $t = 0$, a quantity of free charges Q_f appears on the electrodes of the piezoactuator. At $t = 0+$, after the complete strain of the material is reached, the polarization becomes $P_o + \Delta P$ and the thickness increases to $h + \Delta h$.

To keep the voltage constant, some additional free charges are added by the voltage supply (schematically represented by one more charge on the extended configuration of Fig. 16). In this voltage control, the quantity of free charges is not maintained. Consequently, the relation between voltage and strain is not linear for the piezoactuator. In the case of a free charge control (see Fig. 16), the charge is maintained constant and the strain is proportional to this quantity as pointed out in (26).

The principle of the charge control [see Fig. 17(a)] has been proposed by Comstock [20] and used for a stack by Main [21]. In this work, it is demonstrated that the charge in a piezoactuator obeys the equation: $Q_{\text{pzt}} = C_{\text{ref}} \cdot V_e$. Newcomb [22] proposes a solution based on the constant current integration within a given time t to obtain a charge amount: $Q_{\text{pzt}} = I \cdot t$,

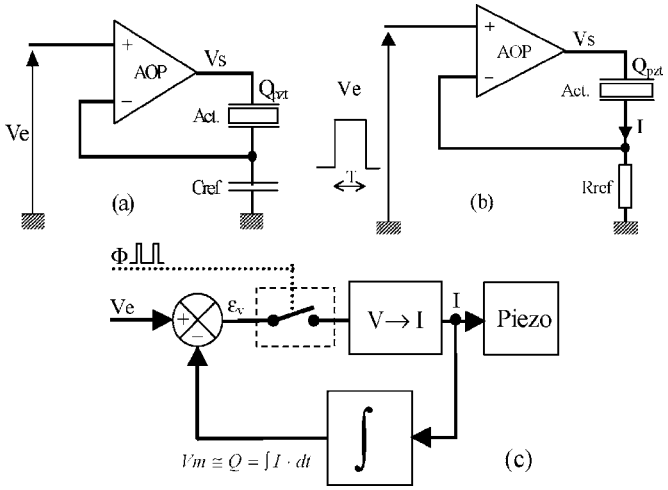

Fig. 17. Different control implementations to achieve a constant quantity of charge on the electrodes of the actuator.

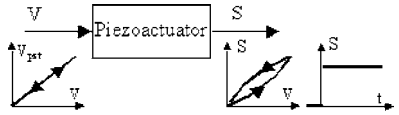

Fig. 18. Voltage control: strain S stable in time, but the transfer between S and V is nonlinear.

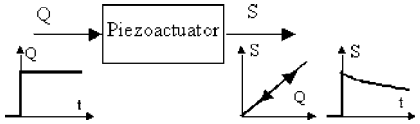

Fig. 19. Charge control: linear transfer between S and Q, but discharge of the actuator.

where $I = V_e/R_{\text{ref}}$ [Fig. 17(b)]. Newton [23] improves this principle by measuring the amount of charge through an integrator [Fig. 17(c)]. Janocha [24], [25], presents a technical solution equivalent to the previous one but the current integration is measured by means of a software structure.

B. Control Q/V

Two major difficulties have to be overcome when working with methods in constant voltage and constant charge.

1) Voltage control of piezoactuators presents a hysteresis between the applied voltage and generated deformation (see Fig. 18). The main difficulty is to make this control linear.
2) Charge control of piezoactuators can result in position drift as the charge dissipates (see Fig. 19). The time constant of the discharge depends on the piezoactuator and goes from some hundreds of milliseconds to tens of seconds. The problem to be solved is how to avoid the loss of charges.

This section presents the principle of the Q/V control developed by the authors. This control allows a static linear behavior in open loop between the deformation of a piezoactuator and its control signal. A hybrid control in charge and voltage is used for this purpose. The resulting control takes advantage of the best features of each of these two control methods.

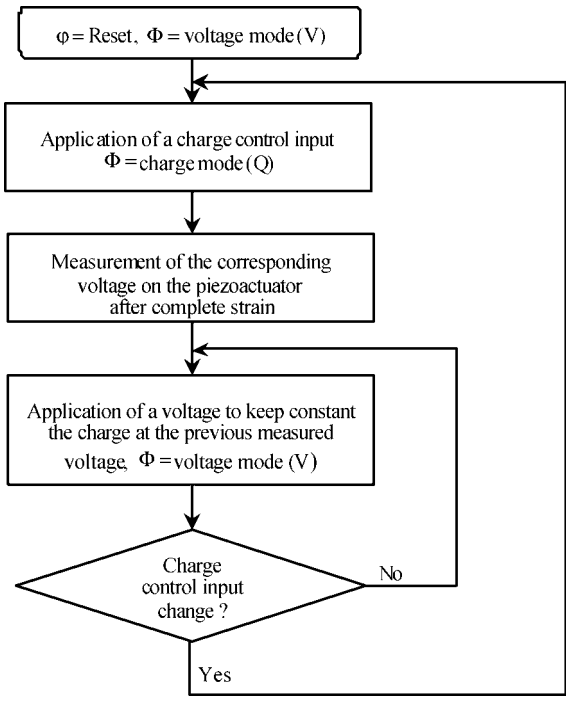

Fig. 20. Flow chart of the Q/V control using a combination of voltage and charge control method.

Fig. 20 shows the working principle of the Q/V control in a flow chart. Four steps are considered in this approach.

1) Application of a quantity of charges to the electrodes of the piezoactuator for a given displacement according to a position control.
2) Measurement of the voltage at the electrodes of the piezoactuator for the quantity of charges applied.
3) Application of a voltage to keep constant the electric charge at the electrodes of the piezoactuator.
4) If the set point is changed, the circuit repeats the three first steps by applying a new quantity of charge. Otherwise, the circuit maintains the charge until a new set value is given.

The implementation of this solution consists of switching in real time from a first configuration to a second one. The first configuration consists of applying a quantity of controlled electric charges to the electrodes of the piezoactuator. The second step consists of applying a continuous voltage corresponding to the charge previously applied. The applied voltage maintains the charge at the desired value.

Fig. 21(a)–(c) show the solution developed in this work. The switching between the charge and voltage controls is made using high-speed CMOS analogical switches I_1 to I_3 controlled by the logic signal Φ. Switch I_4, controlled by φ, is positioned over 'Reset' with $V_c = 0$ and I_1 to I_3 at 'voltage mode' with Φ to define the initial conditions of the device ($V_{\rm PZT} = 0$V, $Q_{\rm ref} = 0$C).

The functional block B_r makes measurements of the output voltage of the amplifier V_s. The latter is mainly composed of a gain G_m to reach V_m that allows the calculation of V_c, i.e., the continuous voltage to apply in order to keep the charge constant through a voltage amplifier (*AOP*, R_1, R_2), as

$$V_c = \frac{V_m}{G_m\left(1 + \frac{R_1}{R_2}\right)}. \tag{27}$$

Fig. 22 compares the free deflection measured using voltage control and Q/V control for a bimorph piezoactuator in z-mode. Voltage control of the piezoactuator gives a hysteresis of 21% for the total amplitude of the deflection. For the Q/V control, the residual hysteresis is reduced to 3.4%. In this example, measurement of V_s is the measure of the quantity of charges $Q_{\rm PZT}$ applied ton the actuator, and the switching from charge control to voltage control is made in a time of 20 ms after the application of the charge.

The Q/V control is particularly suitable within micropositioning applications when we need to keep a constant position but is not well adapted within high dynamic applications like active noise control because of the delay to measure the voltage corresponding to the applied charges.

VIII. Micromanipulation Tests

Micromanipulation is the goal of the MMOC developed at LAB. Training and testing have been carried out with the MMOC in different environments. It has shown the possibilities and limitations of the micromanipulator system.

The MMOC prototype includes duo-bimorphs whose dimensions are 13 mm long, 1 mm wide and 0.4 mm thick. These are integrated into a LEMO connector 43 mm long and 12 mm in diameter from which emerge the useful parts that are in contact with the manipulated objects., i.e., the end-effectors. The end-effectors are 12 mm long and 0.2 mm thick.

The performance of the MMOC is characterized by the following.

1) The measured strokes of open/close motions and up/down motions are 320 and 400 μm, respectively, for $\pm$100 V.
2) The estimated blocking forces on each end-effector tip are 55 mN in gripping (open/close, y direction) and 10 mN in insertion (up/down, z direction) for 100 V. These estimations were obtained using a finite element modeling.
3) The measured first resonance frequency is 1070 Hz for gripping motion and 450 Hz for up and down motion.

One of the environments considered for the training and testing step has been a SEM chamber. One of the advantages of this experience is the possibility of observing with high precision the micromanipulation process. Fig. 23 shows some of these micromanipulation tests developed in a SEM chamber with a MMOC sample.

Manipulation grains in the pictures correspond to a Ni-Co alloy powder. The size of grains ranges from 150 to 200 μm. These dimensions suit the range of displacements of the micromanipulator. Pick-and-place tasks have been carried out in the SEM chamber. The main difficulty to this operation is the coarse approach in z when handling the powder and is the subject of further study.

A crucial point to be regarded in the near future in these pick-and-place operations is the role and the quantification of the adhesion forces. For this, a force sensor is necessary. Force sensors are widely studied at present in microrobotics and automation fields [5]–[7], however, currently, no force sensor has been implemented in the micromanipulation system presented in this section. Much effort is being made at present to permit the integration of a force sensor in the MMOC configuration.

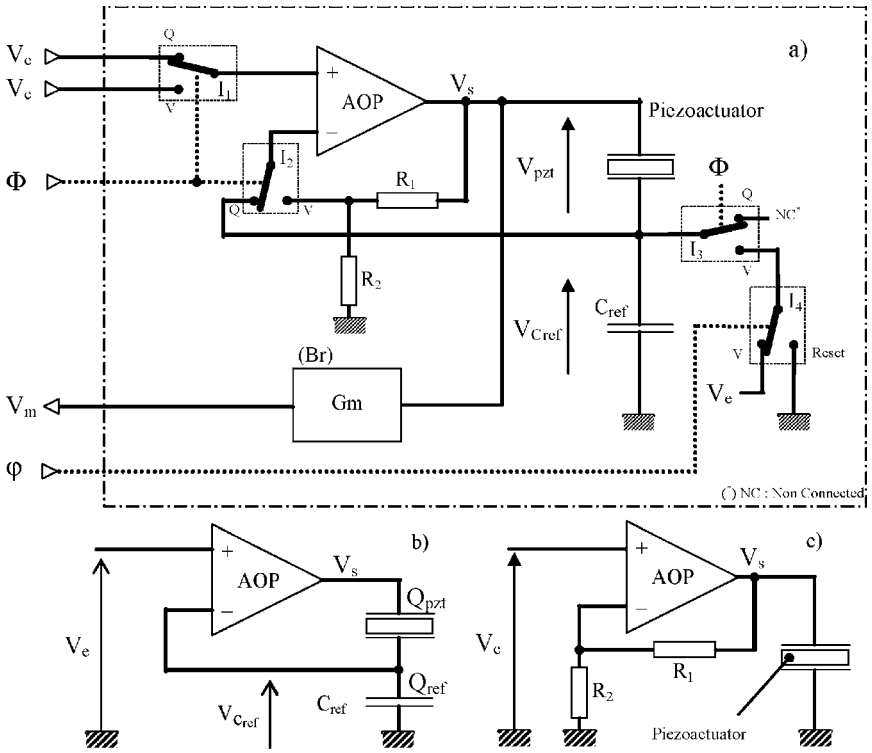

Fig. 21. Solution proposed in this work for the Q/V control of piezoactuators.

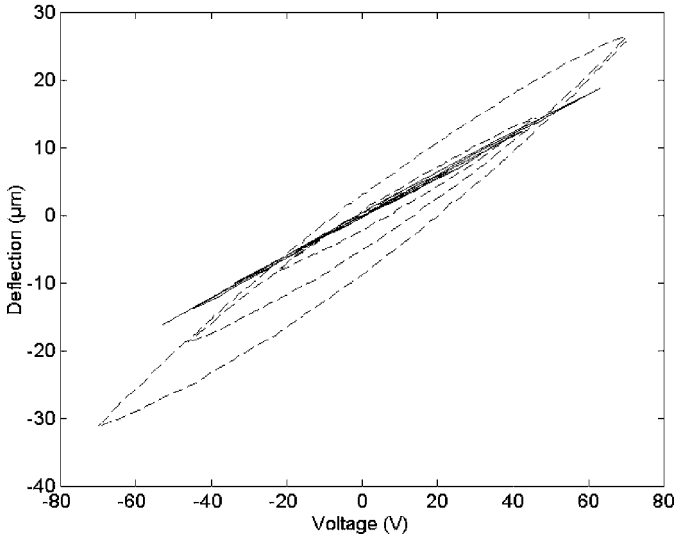

Fig. 22. Different implementations to control a piezoelectric actuator. Dashed lines: voltage control of an actuator with length of 13.5 mm. Solid lines: Q/V control of the same actuator with length of 9 mm.

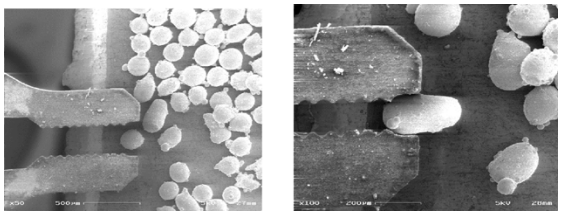

Fig. 23. Micromanipulation of Ni-Co alloy powder in a SEM with the MOC. Powder is from 150 to 200 μm size.

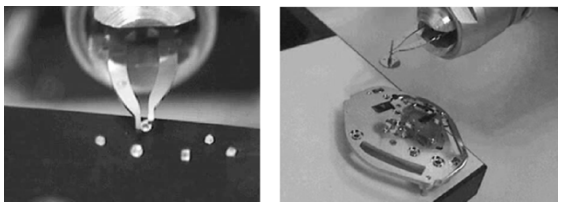

Fig. 24. Micromanipulation of salt grains (left) and watch screw (right) made in the laboratory with the MMOC.

Other examples of manipulation made in the laboratory are shown in Fig. 24. Pick-and-place tasks have been also carried out with salt grains (left) and watch screws (right). Salt grains are typically of some hundreds of microns in size. They present the advantage of being cubic shape and can be easily manipulated by the micromanipulator.

Another interesting test is the manipulation of microobjects such as microcomponents. Fig. 24 right shows the manipulation in pick-and-place of a screw for a watch. In this case the diameter of the screw reaches submillimeter dimensions. As in the previous cases the main limitation of handling is imposed by the optical system. The z-coarse to get near the object before handling is still delicate. Some solutions to this problem are being studied at present.

IX. Conclusion

Micromanipulation feasibility depends highly upon the micromanipulator skills. The MMOC presented in this paper has two main advantages. First is its flexibility to be integrated in other more complex systems such as a micromanipulation platform. Second is its ability to perform micromanipulation tasks.

Models proposed by Smits and de Lit have been applied to the MMOC piezoactuator system. These permit the determination

of different parameters related to the performance of the system including the output displacement. According to the application domain and boundary conditions, scaling of the piezoactuator system such as the duo-bimorph can be made using these models.

The proposed model can be applied to characterize the performance of a duo-bimorph with end-effector. It can also be applied to other systems such as micro positioning or scanning systems. In the case of the micromanipulation, the end-effector is responsible of handling objects. The influence of handling forces is assessed with the model proposed by the authors. According to the results, forces of some tens of milli-Newtons on the end-effectors produce a reduction of 10% in the displacement δ_y of the micromanipulator. Characterization of the MMOC has been made under static and frequency dependent boundary conditions. Displacements in the y- (x-y plane) and z-mode (out of the x-y plane) are 80 and 200 μm at 100 V, respectively. Hysteresis can reach 25% for an open-loop configuration. The first resonance frequency corresponds to a z displacement out from the x-y plane at 400 Hz.

A Q/V control developed by the authors has been implemented. The principle of the Q/V control takes advantage of the charge and voltage controls. It makes the reduction of the hysteresis in a factor of 10 possible. In addition, charges are kept on the electrodes of the piezoactuator. This method does not need a control model and can be consequently applied to any piezoactuator. The only limitation of this method is imposed by the electronics. Parameters necessary for the implementation of this control are the value of the capacity and the response time to a step function of the piezoactuator. These characteristics are easily obtained from the data sheet of the manufacturer and consequently do not represent a limitation on the implementation this control. Finally, the control method presented in this work can be applied to any piezoactuator.

Micromanipulation training and tests have been carried out in a SEM chamber and in the laboratory. Results confirm both the potential applications of the MMOC as well as the difficulties in handling objects, primarily due to the limitation of the optics.

A further step in the design of the MOC micromanipulator is the integration of a force sensor to permit the feedback control during the manipulation.

ACKNOWLEDGMENT

The authors would like to thank the team of the LCEP laboratory, Besançon, France, responsible of the machining of the piezoceramic actuators.

REFERENCES

[1] H. Miyazaki and T. Sato, "Mechanical assembly of three-dimensional microstructures from fine particles," *Adv. Robot.*, vol. 11, no. 2, pp. 169–185, 1997.

[2] H. T. Miyazaki, Y. Tomizawa, K. Koyano, T. Sato, and N. Shinya, "Adhesion force measurement system for microobjects in a scanning electron microscope," *Rev. Scientific Instrum.*, vol. 71, no. 8, pp. 3123–3131, 2000.

[3] K. Koyano and T. Sato, "Micro object handling system with concentrated visual fields and new handling skills," *Proc. SPIE*, vol. 2906, pp. 130–140, 2003.

[4] S. T. Smits and D. G. Chetwynd, "Foundation mechanism design," in *Developments in Nanotechnology*, K. K. Bowen, Ed. Warwick, U.K.: Gordon and Breach Science, 1999, vol. 2.

[5] K. Uchino, *Piezoelectric Actuators and Ultrasonic Motors*, H. L. Tuller, Ed. New York: Academic, 1997.

[6] T. Tanikawa, M. Kawai, N. Koyachi, T. Arai, T. Ide, S. Kaneko, R. Ohta, and T. Hirose, "Force control system for autonomous micro manipulation," in *Proc. IEEE. Int. Conf. Robotics and Automation*, Seoul, Korea, 2001, pp. 610–615.

[7] Y. Shen, N. Xi, W. J. Li, and J. Tan, "A high sensitivity force sensor for microassembly: Design and experiments," in *Proc. IEEE/ASME. Int. Conf. Advanced Intelligent Mechatronics*, vol. 2, 2003, pp. 703–708.

[8] *Piezoelectric Ceramics and Components*, PI ceramic, 1998.

[9] V. Soundararajan and V. Radhakrishnan, "An experimental investigation on the basic mechanisms involved in ultrasonic machining," *Int. Mach. Tool Des. Res.*, vol. 26, no. 3, pp. 307–321, 1986.

[10] S. Ballandras, P. Maître, P. Guine, N. Bourriot, W. Steichen, B. Piranda, and J. F. Gelly, "New results on miniaturised annular arrays built using ultrasound micromachining," in *Proc. IEEE Ultrasonics Symp.*, 1999, pp. 1159–1162.

[11] J. G. Smits, S. I. Dalke, and T. K. Cooney, "The constituent equations of piezoelectric bimorphs," *Sens. Actuators A*, vol. 28, pp. 41–61, 1991.

[12] P. De Lit, J. Agnus, and N. Chaillet, "The constitutive equations of a piezoelectric duo-bimorph," in *Proc. 5th IEEE. Int. Symp. Assembly and Task Planning*, Besançon, France, Jul. 2003, pp. 1–6.

[13] Q.-M. Wang, X.-H. Du, B. Xu, and L. E. Cross, "Electromechanical coupling and output efficiency of piezoelectric bending actuators," *IEEE Trans. Ultras., Ferroelectr., Freq. Contr.*, vol. 46, no. 3, pp. 638–646, Mar. 1999.

[14] *IEEE Standard on Piezoelectricity*, ANSI/IEEE Std. 176, 1998.

[15] R. Pérez, J. Agnus, J.-M. Breguet, N. Chaillet, H. Bleuler, and R. Clavel, "Characterization and control of a 1 DoF monolithic piezoactuator (MPA)," *Proc. SPIE* , pp. 151–162, 2001.

[16] P. Ge and M. Jouaneh, "Tracking control of a piezoceramic actuator," *IEEE Trans. Contr., Syst. Technol.*, vol. 4, no. 3, pp. 209–216, Mar. 1996.

[17] M. Goldfarb and N. Celanovic, "Modeling piezoelectric stack actuators for control of micromanipulation," *IEEE Contr. Syst. Mag.*, vol. 17, no. 3, pp. 69–79, Jun. 1997.

[18] A. J. Fleming and S. O. R. Moheimani, "Improve current and charge amplifiers for driving piezoelectric loads, and issues in signal processing design for synthesis of shunt damping circuits," *J. Intell. Mater. Syst. Structures*, vol. 15, no. 2, pp. 77–92, 2004.

[19] S. O. R. Moheimani, J. Fleming, and S. Behrens, "Dynamics, stability, and control of multivariable piezoelectric schunts," *IEEE/ASME Trans. Mechatron.*, vol. 9, no. 3, pp. 87–99, Mar. 2004.

[20] R. Comstock, "Charge control of piezoelectric actuators to reduce hysteresis effects," U.S. Patent 4 263 527, 1981.

[21] J. Main, E. Garcia, and D. Newton, "Precision position control of piezoelectric actuators using charge feedback," *J.Guidance, Contr. Dynamics*, vol. 18, no. 5, pp. 1068–1073, 1995.

[22] C. Newcomb and I. Flinn, "Improving the linearity of piezoelectric ceramic actuators," *Electron. Lett.*, vol. 18, no. 11, pp. 442–443, 1982.

[23] D. Newton, J. Main, and E. Garcia, "Piezoelectric actuation systems: Optimization of driving electronics," in *Proc. SPIE*, vol. 2717, 1996, pp. 259–266.

[24] H. Janocha, D. Jendritza, and P. Scheer, "Smart actuators with piezoelectric materials," in *Proc. 3rd ICIM/ECSSM Conf.*, 1996, pp. 603–609.

[25] H. Janocha and K. Kuhnen, "Real-time compensation of hysteresis and creep in piezoelectric actuators," *J. Sens. Actuators*, vol. 79, pp. 83–89, 2000.

Ricardo Pérez received the master of physics-astrophysics degree from the University of La Laguna, La Laguna, Spain, in 1993, the postmaster degree in energy systems in 1998, and the Ph.D. degree in microtechnologies in 2002, both from the Ecole Polytechnique Fédérale de Lausanne (EPFL), Lausanne, Switzerland.

He is currently Postdoctoral Researcher at the Laboratoire d'Automatique de Besançon, Besançon, France. His research interests are microactuators, microtecnologies, and modeling of microsystems.

Joël Agnus received the M.S. degree in electrical engineering in 1994 and the Ph.D degree in automatic control and computer sciences from the University of Besançon, Besançon, France, in 2003.

He has been an engineer at the Laboratoire d'Automatique de Besançon, Besançon, France, since 1996. His current research interests are in the microrobotics field and, more particular, in the micromanipulation domain and microgrippers.

Cédric Clévy graduated from the Ecole Normale Supérieure de Cachan, Cachan, France, in 2001 and received the master degree of mechanical engineering, automatics and automation in 2002. He is currently working toward the Ph.D. degree in the Laboratory of Automation of Besançon, Besançon, France.

His research interests are microrobotic, microfactories, and micromanipulation cells using grippers and tools changer

Arnaud Hubert received the engineer diploma in mechanical engineering in 1996, the DEA (M.Sc) degree in system control in 1997, and the Ph.D degree in 2000, all from the University of Technology in Compiegne, Compiegne, France. His Ph.D. research was about noise and vibrations control in electrical drives.

Since 2002, he has been an Assistant Professor at the University of Besançon, Besançon, France, and a Researcher at the Automatic Laboratory in Besancon (LAB), Besançon. His current research interests are the design of microrobotic systems and actuators as well as the control of smart materials.

Nicolas Chaillet received the B.S.E. degree in electrical engineering from the Ecole Nationale Supérieure de Physique, Strassbourg, France, in 1990, and the Ph.D. degree in robotics and automation from the University Louis Pasteur, Strasbourg, France, in 1993.

In 1995, he became an Associate Professor at the University of France-Comté, Besançon, France, working at the Laboratoire d'Automatique de Besançon (LAB). Since 2001, he has been a Professor at the University of Franche Comté and the Head of the LAB Micromanipulation and Microactuators Research Group. His research interests are in microrobotics and, more generally, in micromechatronics fields, especially in micromanipulation, mocrogrippers, smart materials, modeling, and control of microactuators.